Available online at www.sciencedirect.com
SCIENCE DIRECT®

Trans. Nonferrous Met. Soc. China 18(2008) 40−45

Transactions of Nonferrous Metals Society of China

www.csu.edu.cn/ysxb/

Microstructural evolution of aluminum alloy 7B04 thick plate by various thermal treatments

LI Zhi-hui(李志辉), XIONG Bai-qing(熊柏青), ZHANG Yong-an(张永安),
ZHU Bao-hong(朱宝宏), WANG Feng(王　锋), LIU Hong-wei(刘红伟)

State Key Laboratory for Fabrication and Processing of Non-ferrous Metals,
General Research Institute for Non-ferrous Metals, Beijing 100088, China

Received 6 February 2007; accepted 16 July 2007

Abstract: The microstructure of an AA 7B04 alloy in the form of plate was investigated using differential scanning calorimetry (DSC) and TEM analysis technologies. Tensile properties and electrical conductivity of AA 7B04 under various heat treatment conditions were also presented. The results reveal that peak-aged microstructure contains GP zones and η' precipitates predominantly. After retrogressing and reaging(RRA), the η' and η precipitates disperse in the alloy matrix, and the η precipitates distribute coarsely and sparsely, decorating the grain boundaries, together with precipitate free zones(PFZs) around them. It is also shown that selecting of suitable heat treatments can provide optimal precipitates in matrix and at grain boundaries, which gives rise to a combination of high strength and stress corrosion cracking(SCC) resistance in such materials.

Key words: Al alloy; 7B04 aluminum alloy microstructure; TEM; DSC; properties

1 Introduction

The 7000 Al-Zn-Mg-Cu system has been widely studied due to the excellent mechanical properties developed in the alloys after age hardening[1−3]. AA 7B04 (a Chinese brand), a precipitate-age strengthened Al-Zn-Mg-Cu alloy, is a high strength alloy that is used for aircraft structural materials. A large number of researches have been conducted on the mechanisms of zone and precipitate formation in the 7000 series alloys, and models for the decomposition process have been proposed[4−6]. The differential scanning calorimetry (DSC) technique has been used in many regions to characterize the solid state reactions accompanied with the dissolution of precipitates, as well as the formation of additional precipitates. This technique in combination with TEM has been found to be an effective means of studying the precipitation processes in 7000 series alloys[7−10]. Despite of numerous TEM and DSC studies of precipitation in 7000 series alloys, neither the precipitation sequence nor the structure of strengthening phase under various aging conditions are completely clear.

The present work concerns the microstructure in an industrial 7B04 aluminum alloy under various heat treatment conditions. The DSC technique was combined with TEM analysis for this purpose.

2 Experimental

The chemical composition of the alloy tested in the present work is listed in Table 1. The slabs were prepared by traditional ingot metallurgy process. After casting, the slabs were homogenized, scalped, hot-rolled to plates of 40 mm in thickness, solid solution treated at 470 ℃, water quenched (in a roller-type spray quenching equipment) to room temperature, and pre-stretched (residual stress relieving). The bulk samples used in this work were obtained from a monolithic thick plate, and heat treated to T651 (peak aging), T7451 and T7751, i.e. retrogressing and reaging (RRA) tempers. For the T651 temper, the alloy was subjected to a one-step aging involving 22 h at 120 ℃. For the T7451 temper, the alloy was subjected to a two-step aging involving 7 h at 115 ℃ followed by 16 h at 160 ℃. For the RRA temper, the

Foundation item: Project(G2003AA331100) supported by the National High-Tech Research Development Program of China
Corresponding author: ZHANG Yong-an; Tel: +86-10-82241165; E-mail: zhangyongan@grinm.com

Table 1 Chemical composition of 7B04 alloy (mass fraction, %)

Zn	Mg	Cu	Mn	Fe	Si	Ni	Cr	Ti	Al
6.23	2.88	1.58	0.31	0.15	0.048	<0.01	0.16	0.025	Bal.

T651 treated alloy was retrogressed at 180 ℃ for 1 h in a salt bath, water quenched at room temperature followed by reaging to the peak aging condition.

Thermal analysis using DSC was undertaken in a NETZSCH DSC 200 PC instrument using standard methods. The initial microstructure of the as-quenched 7B04 alloy plate was characterized by optical microscopy after specimen preparation with standard metallography and polishing techniques. Microstructural features were revealed by transmission electron microscopy(TEM). TEM specimens were prepared by cutting thin slices from the aged samples, mechanically thinned down to about 50 μm and then electropolished using a twin-jet polisher with a 25% nitric acid solution in methanol at −30−−20 ℃ under an applied voltage of 15−20 V. The foils were examined in JEM 2000FX transmission electron microscope and JEM 2010FX high-resolution electron microscope(HREM). Tensile strength of the thick plate was evaluated in long transverse direction at 1/4 location of the plate thickness using 25 mm gauge length specimens that were pulled in tension with a nominal tension rate of 1 mm/min at room temperature. Electrical conductivity measurement on the samples was carried out using a direct reading type conductivity meter based on eddy current principals.

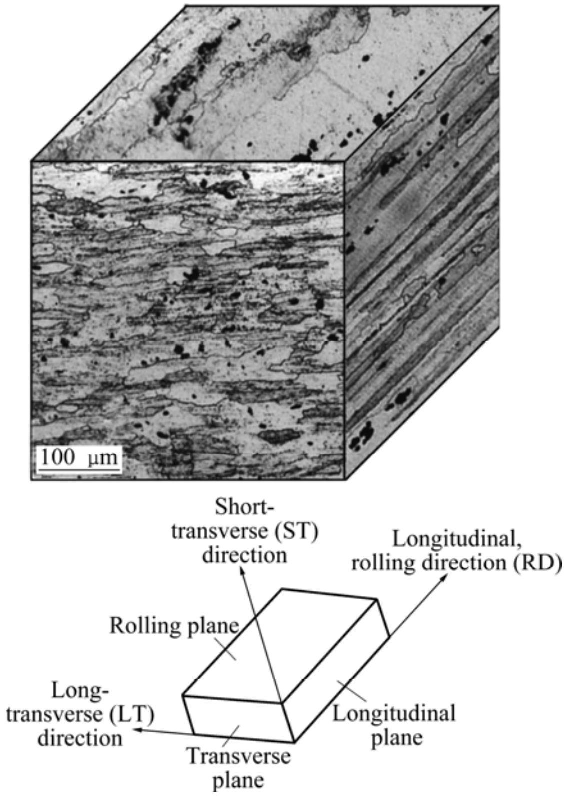

Fig.1 Triplanar optical micrograph illustrating grain morphology of aluminum alloy 7B04 plate

3 Results and discussion

3.1 Microstructure

The microstructure of the as-quenched 7B04 alloy is shown in Fig.1. The triplanar optical micrograph illustrates the grain structure and coarse second-phase particle distribution in the three orthogonal directions of the plate. The microstructure was partially recrystallized with fairly large recrystallized grains that were flattened and elongated in the longitudinal direction, as a direct consequence of the deformation introduced by the rolling operation. Furthermore, the insoluble iron-rich intermetallic particles (Al_7Cu_2Fe) and partially soluble constituent particle (Mg_2Si) were observed to be isolated and randomly distributed along the three orthogonal directions of the as-quenched 7B04 plate. The second-phase particles ranged in size from 0.5 to 5 μm.

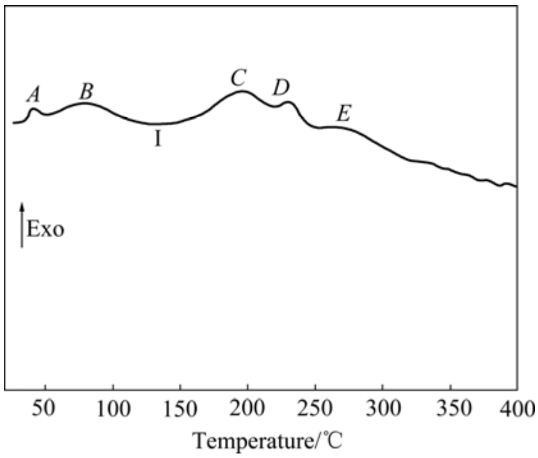

Fig.2 DSC thermogram of 7B04 alloy under as-quenched condition

The DSC thermogram obtained on the 7B04 alloy under as-quenched condition is shown in Fig.2. The principal features of the curve are five exothermic precipitation peaks, *A* (40 ℃), *B* (85 ℃), *C* (195 ℃), *D* (230 ℃), and *E* (280 ℃), and one endothermic dissolution peak, Ⅰ(125 ℃). Most previous published work agrees that two types of zones are deemed in 7000 series alloys, i.e. solute-rich clusters, GP(Ⅰ), which form during low temperature aging, and vacancy-rich clusters, GP(Ⅱ), which form during rapid quenching from the solution treatment temperature. In the present work, two exothermic peaks are clearly defined at temperatures below 130 ℃ labeled as *A* and *B*. It will be shown later that artificial aging T6 produces both GP(Ⅰ) and GP(Ⅱ). It is therefore likely that peak *A* corresponds to the formation of GP(Ⅰ), and peak *B* can be related to the formation or coarsening of GP(Ⅱ) during heating in the DSC. The exothermic peak *C* and *D* are due to the formation of η' and η phase respectively. Furthermore, another exothermic peak, *E*, on the shoulder of the high temperature side of peak *C*, may be due to the nucleation of $T((AlZn)_{49}Mg_{32})$ phase[8]. The presence of endothermic peak, Ⅰ, is due to GP(Ⅱ) transforming into η' while GP(Ⅰ) either dissolves or transforms into η' if it reaches some critical size during a DSC run.

The typical TEM micrograph and SAD pattern of 7B04 alloy under T651 condition is shown in Fig.3. It can be observed that the microstructure of 7B04 alloy consists of very fine precipitates distributed homogeneously in the grain inferior and relatively coarser precipitates distributed continuously on the grain boundaries, without distinct precipitate free zones(PFZs) around them. The presence of GP zones and η' precipitates in the grain inferior was established by analyzing SAD pattern, as shown in Fig.3(b).

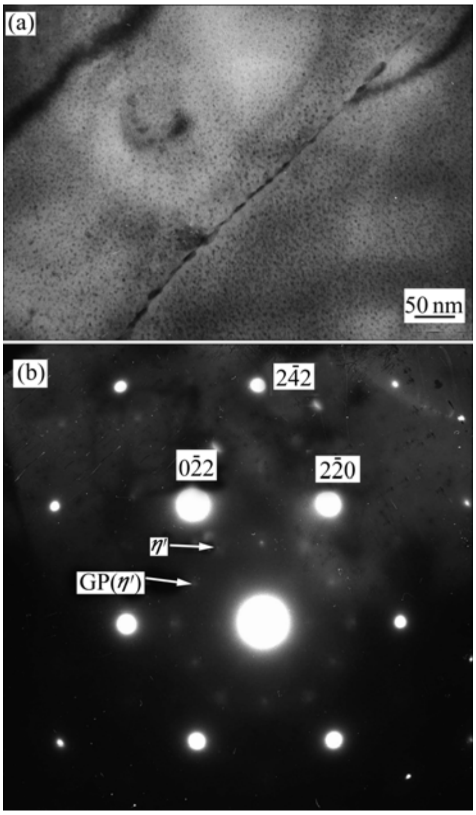

Fig.3 TEM micrograph of 7B04 alloy under T651 condition: (a) Bright field image; (b) SAD pattern taken along $[111]_{Al}$ direction

The DSC thermogram obtained on the 7B04 alloy under T651 condition is shown in Fig.4. The thermogram shows an endothermic peak Ⅱ (200 ℃), and then followed by two exothermic peaks, i.e. peak *D* (230 ℃) and peak *E* (250 ℃). Based on the TEM results and some reported work, interpretation of the DSC curve in Fig.4 can be summarized as follows: 1) endothermic peak Ⅱ is due to the dissolution of unstable η' precipitates and GP zones which coexist in the T651 microstructure; 2) compared with Fig.2, the exothermic reaction of forming η' phase (peak *C* in Fig.2) can not be found in the DSC curve of T651 sample, which therefore confirms that η' phase exists in T651 microstructure; 3) the exothermic peak *D* is due to the formation of η phase. Furthermore, the start melting temperature (approximately 170 ℃) of the precipitates under T651 condition can also be observed in DSC curve.

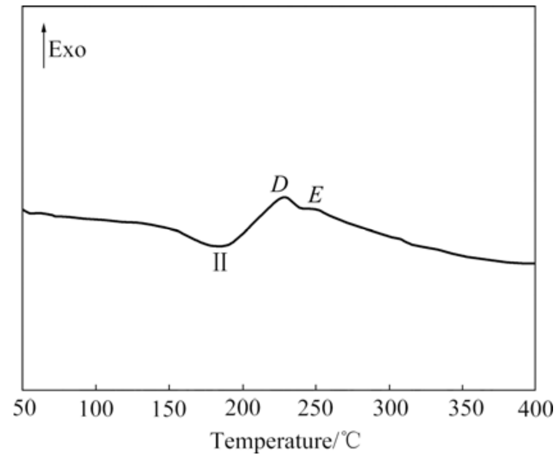

Fig.4 DSC thermogram of 7B04 alloy under T651 aging condition

The typical TEM micrograph and SAD pattern of 7B04 alloy under T7451 condition are shown in Fig.5. From the figure, coarser platelet or rod particles can be seen in the matrix, with their size ranging from 5 to 20 nm. The precipitates in the matrix under this aging condition contain predominantly η' and η phases, and a few retained GPII zones can also be observed. The presence of these phases in the microstructure is established by analyzing SAD pattern and high-resolution transmission electron microscopy(HREM) observations (as shown in Fig.6). Details of the analysis can be found elsewhere[11]. In addition, more sparsely distributed equilibrium η precipitates decorate the grain boundaries (Fig.5(a)), together with precipitate free zones(PFZs) with about 40 nm width around them.

The DSC thermogram obtained on the 7B04 alloy under T7451 condition is shown in Fig.7. The thermogram shows only an endothermic peak Ⅲ, and the peak temperature is higher than that on the curve under T651 aging condition. The endothermic region on the thermogram is due to the dissolution of η' and η phase. The higher peak temperature of this region indicates that the microstructure of T7451 is more stable than that obtained by T651 aging. These results are

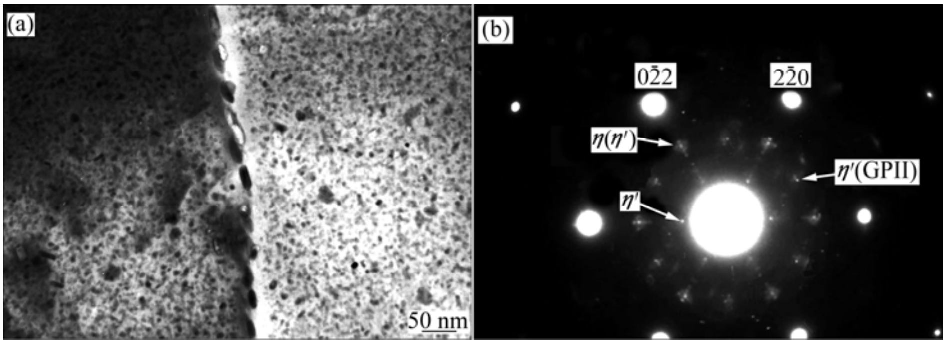

Fig.5 TEM micrographs of 7B04 alloy under T7451 condition: (a) Bright field image; (b) SAD pattern taken along $[111]_{Al}$ direction

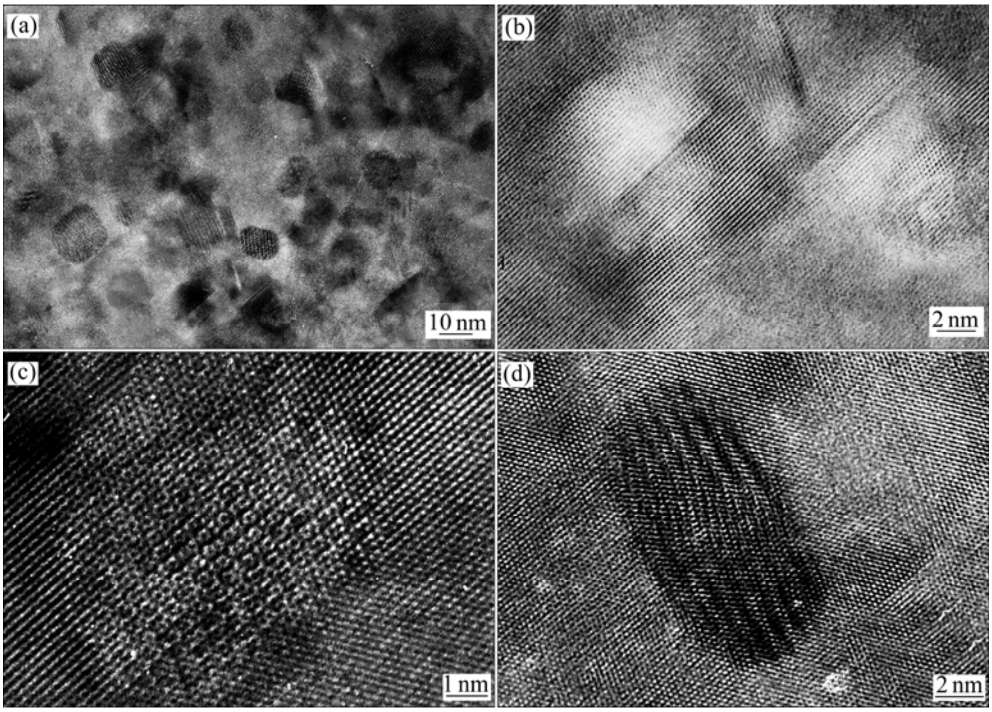

Fig.6 HREM micrographs taken along $[110]_{Al}$ projection of 7B04 alloy under T7451 condition: (a) Relatively low magnification micrograph of precipitates; (b) GP(Ⅱ) zones; (c) Micrograph of η' phase (ring-like contrast, semi-coherent with aluminum matrix); (d) Micrograph of η' phase (rod-like shape, non-coherent with aluminum matrix)

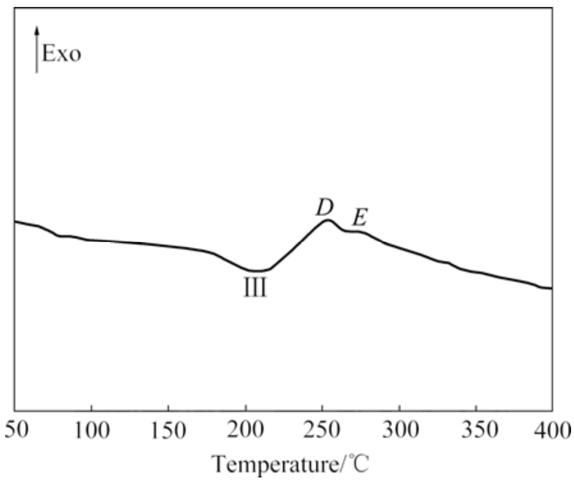

Fig.7 DSC thermogram of 7B04 alloy under T7451 aging condition

consistent with the TEM observations.

Fig.8 illustrates a typical TEM micrograph of 7B04 alloy after being retrogressed at 180 ℃ for 1 h. It can be seen that the density of structural precipitates in the grain interior decreases, and the grain boundary precipitates change to be coarser and more discrete. Based on the DSC results of T651 sample mentioned above and some reported work[12], it can be considered that after retrogression at 180 ℃ for 1 h, some unstable precipitates (GP zones and η' phase) are re-solution treated into the matrix and meanwhile some un-dissolved GP zones and η' precipitates (on both grain interior and boundaries) grow up.

Fig.9(a) shows a TEM micrograph of the alloy after RRA treatment. It can be observed that the precipitates in the matrix are very similar to the T651 microstructure

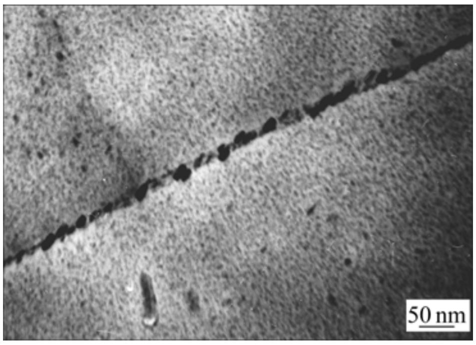

Fig.8 TEM micrograph of 7B04 alloy after retrogression at 180 ℃ for 1 h

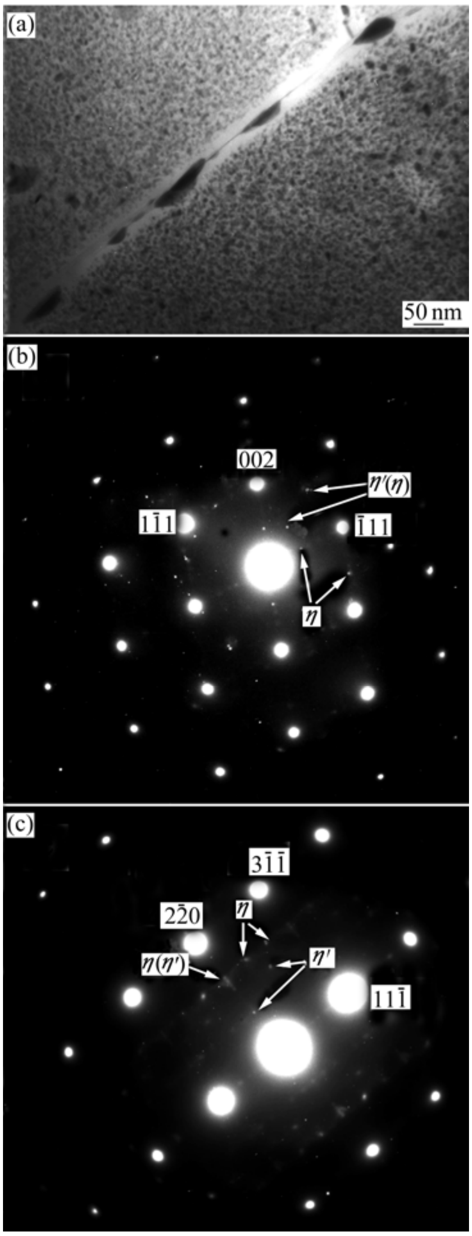

Fig.9 TEM micrographs of 7B04 alloy under RRA condition: (a) Bright field image; (b) SAD pattern taken along $[110]_{Al}$ direction; (c) SAD pattern taken along $[112]_{Al}$ direction

(Fig.3(a)), which are very fine with their size ranging from 5 to 10 nm and distribute homogeneously, and some coarser particles however are presented. Meanwhile, the grain boundary precipitates change to be coarser and more sparsely distributed, and the PFZ with width of 40 nm around the grain boundary can also be observed. The SAD patterns taken along $[110]_{Al}$ and $[112]_{Al}$ projection are illustrated in Figs.9(b) and (c), respectively. The SAD patterns analysis indicates that extra spots are mainly from η' phase and η phase, confirming that the re-precipitation of η' phase occurs during the re-aging process.

Fig.10 shows the DSC thermogram under RRA aging condition. It can be seen that the endothermic reaction (peak Ⅳ) in the thermogram of the alloy under the RRA condition occurs in a temperature range is very close to that under T651 aging condition, which implies that there is no obvious difference in size and density of precipitates in the matrix under RRA and T651 conditions, and this is also confirmed by TEM. As a result, it is not surprising that the tensile strength of the alloy in the RRA temper is very close to that obtained under the T6 aging condition.

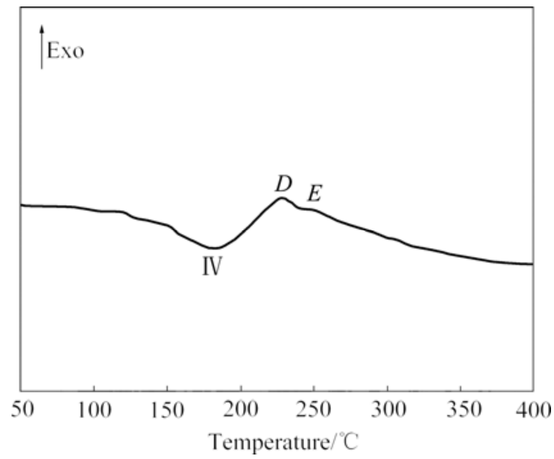

Fig.10 DSC thermogram of 7B04 alloy under RRA aging condition

3.2 Mechanical properties and electrical conductivity

Table 2 presents the tensile properties and the electrical conductivity of 7B04 alloy in various tempers. It may be noted that the differences between tensile properties in peak aged and RRA temper are minimal. On the other hand, the electrical conductivity in the RRA temper (close to the electrical conductivity in T7451 temper) considerably increases compared with that in the peak aged alloy, suggesting improved SCC resistance of RRA treated alloy based on some reported work[13−16] concerning the relationships between electrical conductivity and SCC resistance in 7000 series alloys. These results are consistent with the beneficial effects of the RRA treatment on the microstructure in that it results in the coarsening of matrix precipitates together with the formation of equilibrium precipitates in the matrix. The dislocation-precipitate interaction changes from shearing to bypassing of precipitates, thus homogenizing the slip. The coarse, sparse grain boundary precipitates increase, thus providing resistance against stress corrosion cracking; and the corrosion potential gradient between the matrix and the grain boundary regions is reduced, thus reducing the selective corrosion[17−18].

Table 2 Tensile properties and electrical conductivity of 7B04 alloy thick plate under various heat treated conditions

Condition	Ultimate strength/ MPa	Yield strength/ MPa	Elongation/ %	Electrical conductivity/ ($MS \cdot m^{-1}$)
As-quenched	395	206	23.9	14.3
T651	595	534	11.5	18.3
T7451	523	445	10.5	21.8
Retrogressed at 180 ℃ for 1 h	566	496	12.0	19.5
RRA (Retrogressed at 180 ℃ for 1 h)	583	522	10.0	21.0

4 Conclusions

1) The AA7B04 alloy has a partially recrystallized microstructure with the large recrystallized grains flattened and elongated in the longitudinal direction. The coarse second-phase particles and partially soluble constituent phases are observed to be isolated and randomly distributed along the three orthogonal directions of the rolled plate.

2) During the decomposition of the supersaturated solid solution of AA 7B04, two types of cluster, GP(Ⅰ) and GP(Ⅱ) zones are formed.

3) T651 ageing gives the largest strengthening effect due to the dominant formation of GP zones and η' phase homogeneously distributed in the matrix.

4) In RRA treated microstructure, the η' and η precipitates disperse in the alloy matrix, and coarser and sparsely distributed η precipitates decorate the grain boundaries, together with precipitate free zones (PFZs) with about 40 nm in width around them.

References

[1] FRIDLYANDER I N, DOBROMYSLOV A V, TKACHENKO E A, SENATOROVA O G. Advanced high-strength aluminum-base materials [J]. Met Sci Heat Treat, 2005, 47(7/8): 269−275.

[2] WANG F, XIONG B Q, ZHANG Y A, ZHANG Y A, WANG Z X, ZHU B H, LIU H W. Microstructure and mechanical properties of spray-deposited Al-Zn-Mg-Cu alloy [J]. Mater Design, 2007, 28(4): 1154−1158.

[3] WARREN A S. Developments and challenges for aluminum—A boeing perspective [C]// Proc 9th Int Conf Aluminium Alloys, Australia: Institute of Materials Engineering Australia Ltd., 2004: 24−31.

[4] KVERNELAND A, HANSEN V, VINCENT R, GJ∅NNES K, GJ∅NNES J. Structure analysis of embedded nano-sized particles by precession electron diffraction η'-precipitate in an Al-Zn-Mg alloy as example [J]. Ultramicroscopy, 2006, 106: 492−502.

[5] WERENSKIOLD J C, DESCHAMPS A, BRECHET Y. Characterization and modeling of precipitation kinetics in an Al-Zn-Mg alloy [J]. Mater Sci Eng, 2000, A293: 267−274.

[6] GANG S, ALFRED C. Early-stage precipitation in Al-Zn-Mg-Cu alloys (7050) [J]. Acta Mater, 2004, 52: 4503−4516.

[7] RIONTINO G, DUPASQUIER A, FERRAGUT R, IGLESIAS M M, MACCHI C, MASSAZZA M, MENGUCCI P, SOMOZA A. Formation and morphology of hardening nanostructures in an AlZnMg alloy [C]// Proc 9th Int Conf Aluminium Alloys, Australia: Institute of Materials Engineering Australia Ltd., 2004: 652−658.

[8] MUKHOPADHYAY A K, YANG Q B, SINGH S R. The influence of zirconium on the early stages of aging of a ternary Al-Zn-Mg alloy [J]. Acta Metal Mater, 1994, 42(9): 3083−3091.

[9] JIANG X J, NOBLE B, HANSEN V, TAFTO J. Influence of zirconium and copper on the early stages of aging in Al-Zn-Mg alloys [J]. Metall Mater Trans A, 2001, 32A: 1063−1073.

[10] GARCIA-CORDOVILLA C, LOUIS E. A differential scanning calorimetry investigation of the effects of zinc and copper on solid state reactions in Al-Zn-Mg-Cu alloys [J]. Mater Sci Eng, 1991, A132: 135−141.

[11] LI Z H, XIONG B Q, ZHANG Y A, ZHU B H, WANG F, LIU H W. Investigation of microstructural evolution and mechanical properties during two-step ageing treatment at 115 ℃ and 160 ℃ in an Al-Zn-Mg-Cu alloy pre-stretched thick plate [J]. Mater Char, 2008, 59(3): 278−282.

[12] DANH N C, RAJAN K, WALLACE W. A TEM study of microstructure changes during retrogression and reaging in 7075 aluminum [J]. Metall Trans, 1983, 14A: 1843−1850.

[13] DENZER D K, CHAKRABARTI D J, LIU J, OSWALD L E, WESTERLUND R W. Method for increasing the strength and/or corrosion resistance of 7000 series Al aerospace alloy products [P], US 20030051784, 2003.

[14] FERRER C P, KOUL M G, CONNOLLY B J, MORAN A L. Improvements in strength and stress corrosion cracking properties in aluminum alloy 7075 via low-temperature retrogression and re-ageing heat treatments [J]. Corros Sci, 2003, 59(6): 520−528.

[15] ZHU B H, ZHANG Y A, XIONG B Q, LI Z H, WANG F, LIU H W. Effect of artificial aging temper on the microstructure and properties of 7B04 pre-stretched thick plate [J]. Materials Science Forum, 2006, 519/521: 901−905.

[16] SALAZAR-GUAPURICHE M A, ZHAO Y Y, PITMAN A, GREENE A. Correlation of strength with hardness and electrical conductivity for aluminium alloy 7010 [J]. Materials Science Forum, 2006, 519/521: 853−858.

[17] LUKASAK D A, HART R M. Strong aluminium alloy shaves airframe weight [J]. Light Metal Age, 1991, 49(5): 11−15.

[18] PUIGGALI M, ZIELINSKI A, OLIVE J M, RENAULD E, DESJARDINS D, CID M. Effect of microstructure on stress corrosion cracking of an Al-Zn-Mg-Cu alloy [J]. Corros Sci, 1998, 1998, 40(4/5): 805−811.

(Edited by LI Xiang-qun)